Improved retention of phosphorus donors in germanium using a non-amorphizing fluorine co-implantation technique

As Published: 10.1063/1.4999210

Publisher: AIP Publishing

Persistent URL: https://hdl.handle.net/1721.1/134690

Version: Final published version: final published article, as it appeared in a journal, conference proceedings, or other formally published context

Improved retention of phosphorus donors in germanium using a non-amorphizing fluorine co-implantation technique

Corentin Monmeyran, Iain F. Crowe, Russell M. Gwilliam, Christopher Heidelberger, Enrico Napolitani, David Pastor, Hemi H. Gandhi, Eric Mazur, Jürgen Michel, Anuradha M. Agarwal, and Lionel C. Kimerling

Citation: Journal of Applied Physics **123**, 161524 (2018);
View online: https://doi.org/10.1063/1.4999210
View Table of Contents: http://aip.scitation.org/toc/jap/123/16
Published by the American Institute of Physics

Improved retention of phosphorus donors in germanium using a non-amorphizing fluorine co-implantation technique

Corentin Monmeyran,[1] Iain F. Crowe,[2] Russell M. Gwilliam,[3] Christopher Heidelberger,[1] Enrico Napolitani,[4] David Pastor,[5] Hemi H. Gandhi,[5] Eric Mazur,[5] Jürgen Michel,[6] Anuradha M. Agarwal,[6] and Lionel C. Kimerling[1,6]

[1]*Department of Materials Science and Engineering, Massachusetts Institute of Technology, 77 Massachusetts Ave., Cambridge, Massachusetts 02139, USA*
[2]*Photon Science Institute and School of Electrical and Electronic Engineering, University of Manchester, Manchester M13 9PL, United Kingdom*
[3]*Ion Beam Centre, University of Surrey, Guildford, Surrey GU2 7XH, United Kingdom*
[4]*Dipartimento di Fisica e Astronomia, Università di Padova and CNR-IMM, Via, Marzolo 8, Padova I-35131, Italy*
[5]*Harvard John A. Paulson School of Engineering and Applied Sciences, Cambridge, Massachusetts 02138, USA*
[6]*Microphotonics Center, Massachusetts Institute of Technology, 77 Massachusetts Ave., Cambridge, Massachusetts 02139, USA*

(Received 6 August 2017; accepted 6 October 2017; published online 1 November 2017)

Co-doping with fluorine is a potentially promising method for defect passivation to increase the donor electrical activation in highly doped n-type germanium. However, regular high dose donor-fluorine co-implants, followed by conventional thermal treatment of the germanium, typically result in a dramatic loss of the fluorine, as a result of the extremely large diffusivity at elevated temperatures, partly mediated by the solid phase epitaxial regrowth. To circumvent this problem, we propose and experimentally demonstrate two *non-amorphizing* co-implantation methods; one involving consecutive, low dose fluorine implants, intertwined with rapid thermal annealing and the second, involving heating of the target wafer during implantation. Our study confirms that the fluorine solubility in germanium is defect-mediated and we reveal the extent to which both of these strategies can be effective in retaining large fractions of both the implanted fluorine and, critically, phosphorus donors. *Published by AIP Publishing*. https://doi.org/10.1063/1.4999210

INTRODUCTION

Achieving high free electron concentrations in germanium is critical for the fabrication of next generation, CMOS integrated microelectronic and optoelectronic devices such as lasers and MOSFETs.[1,2] However, for high chemical concentrations of incorporated donors, saturation of the free carrier concentration, in the mid 10^{19} cm^{-3} range, is generally observed for a wide range of doping methods[3–9] and it is widely accepted that this is due to binding of the donors to point defects to form donor-vacancy (D_nV_m) complexes.[10–12] These complexes transform substitutional donors into donor compensating multi-acceptors,[13–16] which leads to an incomplete activation of the implanted donors. Multiple strategies have been proposed to overcome this issue with some, albeit limited, success.[17,18] One possible approach that has not been fully explored is the co-implantation of fluorine and donors, with the explicit intention of leveraging the high electronegativity of fluorine to preferentially complex with vacancies present in the material, thus neutralizing their effect on the donors.[19] Density Functional Theory (DFT) calculations[20] indicate that the binding energy of a fluorine-vacancy (FV) complex is significantly higher than the donor vacancy (DV) complexes, while the formation of fluorine-donor complexes is considered highly unlikely (in contrast with the case of nitrogen[21] and carbon co-doping[22]). This approach is therefore expected to significantly improve the donor electrical activity through both reduced DV complex formation and retarded diffusivity (donor diffusion is vacancy-assisted). However, in spite of previous efforts,[23–28] practical implementation of this has not yet been realized because of the efficient out-diffusion of the fluorine, mediated by the Solid Phase Epitaxy (SPE) during high temperature treatments following implantation.[26] SPE is the phenomenon by which crystallinity is recovered (and donors are properly incorporated at substitutional lattice sites) after the (amorphizing) co-implantation of donors and fluorine. The issue is that the fluorine tends to segregate at the amorphous/crystalline interface during this regrowth[26] and is effectively 'pushed' out of the material. There are essentially two ways to try to circumvent this: (i) by employing a sub-second solidification technique, i.e., using pulsed laser annealing (the dynamics of conventional Rapid Thermal Annealing (RTA) are insufficient in achieving this) to increase the recrystallization rate well beyond that of the fluorine diffusion at the re-growth front,[29] or (ii) by avoiding SPE altogether through the use of a *non-amorphizing* implant,[19] which is the approach explored in this contribution. We examine two different *non-amorphizing* implant schemes that can circumvent this issue and, in doing so, we are able to decouple the fluorine profiles from the SPE and instead show that they are governed by the distribution of point defects in the material.

Ion beam induced amorphization occurs when the number of point defects introduced by the implantation exceeds a certain threshold, the *Critical Point Defect Density*[30] ($\sim 3 \times 10^{21}$ cm^{-3} for Ge[31]). The number of vacancy type defects

introduced by ion implantation of a target substrate with a particular species can be estimated using the Stopping and Range of Ions in Matter (SRIM) Monte-Carlo simulation program.[32] For shallow implants and fluorine doses sufficient to obtain concentrations of $\sim 10^{19}\,cm^{-3}$, amorphization always occurs for 'regular' implant conditions (i.e., single dose delivery at room temperature). However, we describe two novel approaches to achieve high concentrations of fluorine without amorphizing the germanium: (1) via consecutive, low dose fluorine implants, intertwined with RTA, which partially suppresses cumulative damage 'build-up' (we refer to this as "intertwined" implantation), or (2) by implanting into a 'hot' (200 °C) wafer, which has the effect of increasing the dynamic annealing of the *Frenkel* pairs resulting in a lower rate of vacancy defect generation[33] (we refer to this as "hot wafer" implantation).[19]

EXPERIMENTAL

For both techniques, initial sample preparation was identical; thin germanium layers were grown epitaxially on a p-type silicon wafer by Ultra High Vacuum Chemical Vapor Deposition (UHVCVD), using a two-step method described previously.[34] The germanium was then capped by a 30 nm layer of CVD grown SiO_2, which is a standard technique for minimizing donor out-diffusion during annealing. We then employ a 900 keV, $10^{14}\,cm^{-2}$ dose germanium (self-) pre-amorphization implant (PAI), giving a projected range, $R_P = 440$ nm. This step has been found to provide a systematic improvement in the final free carrier concentration, via differential *Hall* measurements (not shown here). The samples were then implanted with phosphorus at 200 keV to a dose of $5 \times 10^{15}\,cm^{-2}$, which gives a projected range, $R_P = 160$ nm below the Ge/oxide interface with a peak phosphorus concentration close to the solid solubility limit of $2 \times 10^{20}\,cm^{-3}$.[35] This was followed with a single RTA cycle at 600 °C for 2 s (preceded by a 25 s ramp-up from room temperature and followed by a 260 s cool-down to 100 °C after lamp switch off) to recover their crystallinity by SPE. Finally, we incorporated the different "intertwined" or "hot wafer" fluorine implants. The intertwined samples were implanted with fluorine in steps of $5 \times 10^{13}\,cm^{-2}$ with 2 s, 600 °C RTA between each step. For the hot wafer sample the fluorine implant was conducted with the wafer heated to 200 °C, followed by a 2 s, 600 °C RTA to remove implantation damage. During the hot wafer implants, for the fluorine implanted dose of 4×10^{14} ions cm^{-2}, the dose rate was 3×10^{11} ions $cm^{-2}\,s^{-1}$, taking 21 min to complete, and for the implanted dose of 1×10^{15} ions cm^{-2}, the dose rate was 5×10^{11} ions $cm^{-2}\,s^{-1}$, taking 32 min to complete. We examined the effects of both different cumulative concentrations of fluorine and implant energy; either 120 keV to match the phosphorus projected range (160 nm) or 150 keV to give a peak concentration of fluorine at ~200 nm, i.e., just beyond the phosphorus implant peak. XTEM micrographs (not shown here) revealed that the sample crystallinity was preserved after the fluorine implantation using both methods. Control samples were also prepared from the same germanium and phosphorus implants, without fluorine, and employing single cycle RTA at 600 °C for 2 s.

In order to separate any chemical effect of fluorine retention via complex formation with phosphorus (i.e., formation of fluorine-donor complexes), from that of defect passivation by fluorine (i.e., through FV complex formation), we also examined the retained fluorine fraction in samples pre-implanted with nitric oxide (NO) dimers (instead of phosphorus). The NO dimer has a similar mass to phosphorus and thus yields a similar implantation damage, while having different chemical properties.

RESULTS

The fluorine profiles after a final RTA (2 s, 600 °C) anneal, shown in Fig. 1, are atypical. Despite the *non-amorphizing* nature of the implants and hence absence of SPE regrowth during annealing, we note that the level of fluorine retention is still below 10% (as calculated from the secondary ion mass spectrometry (SIMS) profiles), indicative of strong out-diffusion. Furthermore, three features from all the SIMS profiles are striking: the profile asymmetry, a relative independence of the profile on implantation energy, and a non-linear increase of the concentration with implanted dose. These properties of the fluorine profiles are a consequence of the low solubility of this element in *crystalline* germanium and evidence the fact that the solubility of fluorine is mediated by point defects, as we will show. In the case of standard, isotropic diffusion, chemical profiles broaden symmetrically. The asymmetry of the fluorine profiles observed here shows that the fluorine spread is anisotropic, concentrated in the region between the surface and the implantation peak position (i.e., in the first 200 nm, where the implantation damage is highest). The origin of this asymmetry can be due to either a diffusion gradient or a

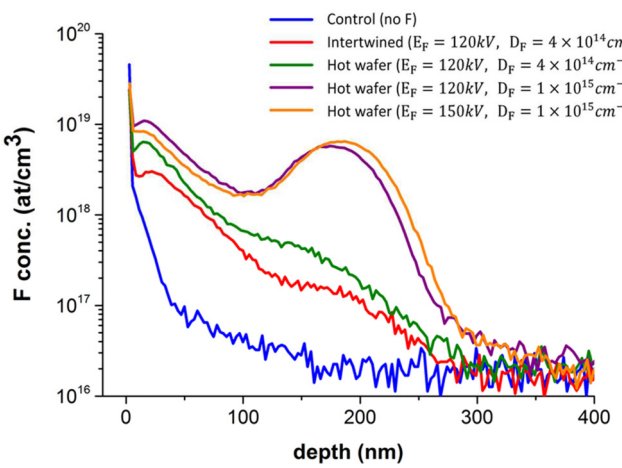

FIG. 1. Post RTA fluorine SIMS profiles of an 'intertwined' and various 'hot wafer' implants (two different fluorine doses and implant energies). Data for a control wafer (no fluorine) are included to illustrate the sensitivity limit of the SIMS measurement ($\sim 2 \times 10^{16}\,cm^{-3}$). The projected fluorine ranges for $E_F = 120$ keV and 150 keV are 160 nm and 200 nm, respectively. Note the skewing of all the profiles toward the surface region and the concentration build-up at the implantation peak for the highest fluorine doses, as a result of the higher solubility of fluorine in the more defect-rich regions. The concentration build up at the near surface region (~25 nm) in all the samples is due to the oxide cap.

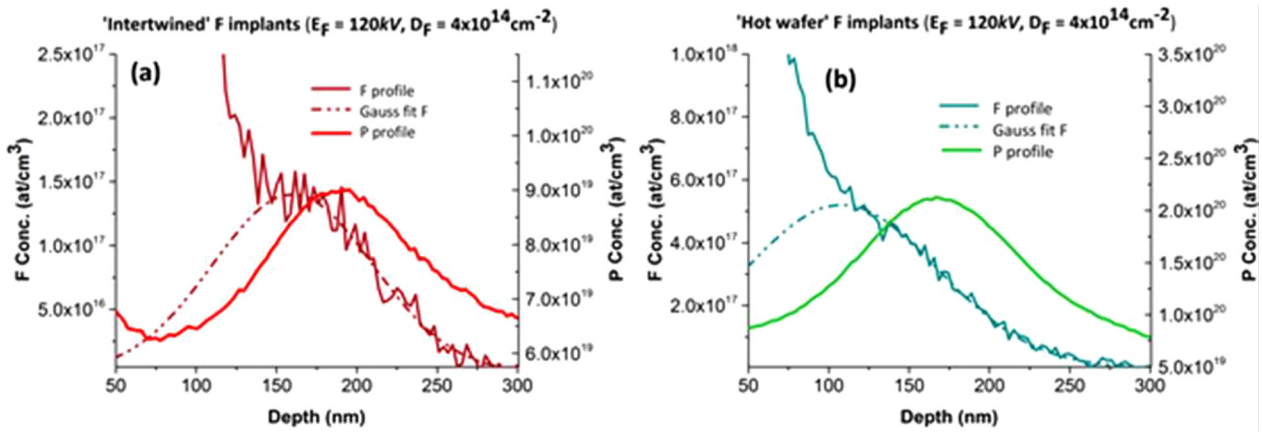

FIG. 2. Post-RTA phosphorus (right axes) and fluorine (left axes) SIMS profiles (linear scale) around the implantation peak positions: (a) Intertwined and (b) hot wafer fluorine implants at 120 keV to a dose of 4×10^{14}cm^{-2}.

solubility gradient between the high quality crystalline phase (beyond 200 nm) and the defective phase closer to the surface. In addition to the high level of fluorine outgassing to the implanted surface, we also observed that a significant fraction of the fluorine had diffused throughout the germanium epitaxial layer, towards the rear interface with the silicon substrate, as shown in Fig. 5, and discussed in the "Conclusions" section of this contribution. Given the dynamics of the annealing, this suggests an exceptionally large diffusivity even in the pristine crystalline phase and indicates that the observed profile asymmetry is rather the result of a large solubility difference. Because it is most soluble in defective regions, the fluorine distribution tracks the point defect distribution, whose asymmetry is of course due to the asymmetry of the implantation: most defects are generated between the surface and the implantation peaks, and no defect is generated past the end-of-range.

The higher solubility of fluorine in this region is also confirmed by the relative insensitivity of the fluorine profiles to the implantation energy (depth). For the two 'hot wafer' samples implanted with the highest fluorine dose (10^{15} cm^{-2}) but at different energies, Fig. 1 violet (120 keV/160 nm) and green (150 keV/200 nm) curves, despite a fairly significant depth difference of the implantation peaks (~40 nm), have very similar post-RTA profiles (the stochastic nature of implantation typically yields much wider profiles with lower peak concentrations as the energy for a given implanted species increases). We attribute this implant energy (or depth) insensitivity to the fact that, due to its high diffusivity, fluorine quickly goes where it is most soluble, i.e., regions with higher defect concentrations, which effectively attract and 'pin' the fluorine. This is the case around the phosphorus implantation peak. Indeed, correlation of a high concentration of vacancy defects with high concentrations of implanted donors, generally, explains the incomplete electrical activation of the donors that is often reported for concentrations in excess of $\sim 5 \times 10^{19}$ cm^{-3}, through a self-compensation mechanism. We rule out the possibility that fluorine is forming complexes with the phosphorus however because the highly asymmetric fluorine profiles differ significantly from the more symmetric phosphorus profiles, as confirmed by Fig. 2. The fluorine tracks point defects, not phosphorus.

Comparison of the intertwined and hot wafer samples, both implanted with fluorine at 120 keV to 4×10^{14} cm^{-2}, Figs. 2(a) and 2(b), reveals a higher (~factor of 3) retained fluorine in the latter, with a correspondingly higher fraction (~factor of 2.5) of retained phosphorus. This indicates that the fluorine solubility is higher (lower outgassing) in the hot wafer sample, presumably as a result of a higher remnant defect concentration. This is either because of a higher defect generation rate in the hot wafer sample or more effective removal of the defects in the intertwined sample due to a higher thermal budget. The implantation method thus impacts the fluorine retention. The dose also has an influence: the defect profiles do not scale linearly with dose, even for the same implantation method, as shown in Fig. 1 for hot wafer samples. Even if there is no large build-up of fluorine at the projected range (~160 nm) for the lowest doses of fluorine, the fluorine distributions for the highest fluorine doses have a local maximum at the P peak location, which is also where the defect concentration peaks. This threshold effect is most likely due to the generation of larger defects in the germanium once a certain dose of fluorine has been implanted. The crystalline material indeed does not pass suddenly from a purely crystalline phase to a purely amorphous phase when the Critical Point Defect Density is reached. When the implantation dose increases, the number of defects and their size increases continuously, and so does the defect-mediated fluorine solubility. Once the solubility is high enough that the fluorine does not immediately diffuse away, one might expect a buildup of fluorine, as we have observed.

The presence of F also impacts the P distribution. The difference in the P profiles between the hot wafer samples and the control wafer in Fig. 3 is only partly due to their thermal budget. By design, the hot wafer samples have all undergone a higher thermal budget than the control wafer (two RTA cycles at 600 °C versus one for the control wafer, in addition to the 200 °C treatment during the fluorine implant), which implies that the phosphorus profile should be broader in the hot wafer than in the control sample. This was the case for the samples implanted with the lowest dose of

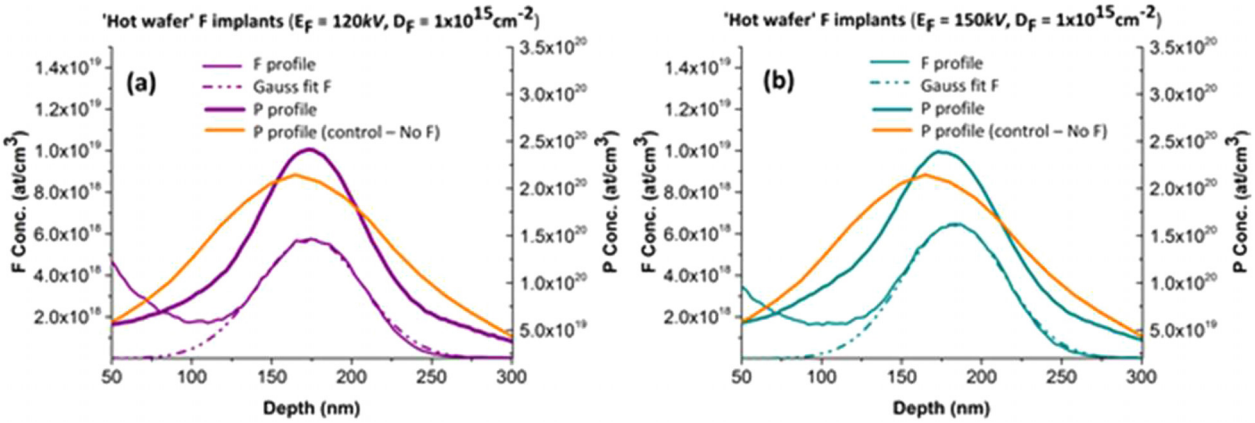

FIG. 3. Post-RTA phosphorus (right axes) and fluorine (left axes) SIMS profiles (linear scale) around the implantation peak positions for hot wafer fluorine implants at (a) 120 keV and (b) 150 keV to a dose of 1×10^{15}cm^{-2}. The phosphorus profile for the control (no fluorine) sample is shown in both figures for comparison.

fluorine (4×10^{14} cm^{-2}). However, at the implantation peak for the highest dose of fluorine (10^{15} cm^{-2}), the pinching of the phosphorus distribution (Fig. 3) suggests that the phosphorus diffusion is suppressed, where the fluorine concentration is the highest, and that this effect counters the higher thermal budget. We interpret it as the fact that the fluorine dose of 10^{15} cm^{-2} is sufficient to passivate a large fraction of the vacancy population around the implantation peak such that fewer vacancies participate in DV complex formation, which would normally enhance phosphorus diffusion (and ultimately lead to higher loss). There appears therefore to be a threshold fluorine dose effect beyond which the passivation of a sufficiently large fraction of vacancies suppresses the most effective phosphorus diffusion pathway.

Figure 4 provides further evidence that the solubility of fluorine is mediated by point defects. The fluorine SIMS profiles in samples pre-implanted with NO-dimers (rather than phosphorus), before and after the final RTA, have been superimposed onto cross-sectional TEM images for intertwined and hot wafer samples (after final RTA).

The dark elongated regions correspond to point defects that remain after the SPE, and are more numerous in the intertwined sample. The 100 nm wide horizontal shadows are artefacts of the diffraction conditions (g = (220)). In these two samples, nitric oxide (NO) dimers were incorporated instead of phosphorus (with identical energy, dose, and RTA conditions) prior to the *non-amorphizing* fluorine implants. The NO dimer has a similar mass to phosphorus and thus approximately yields a similar implantation damage, while having different chemical properties. In particular, theoretical[36,37] and experimental[21,22,38] studies have shown that they readily complex with vacancies; their presence results in more defective layers after the SPE. The implantation energy of fluorine in these samples is 120 keV (same as that in Fig. 1), but the dose is lower, at 2×10^{14} cm^{-2}. The retained fluorine concentration (post-RTA) is higher in these more defective samples (52% for the "intertwined", 15% for the "hot wafer") than in those pre-implanted with phosphorus (10%). This is because the O and N have indeed stabilized point defects during the SPE: this confirms further that the F solubility is point defect mediated. Furthermore, despite similar as-implanted profiles, the post-RTA fluorine distributions in these two samples vary widely between the intertwined and the hot wafer sample, because of different initial point defect concentrations. As expected, the micrograph shows that the most defective sample (the intertwined) also has the highest retention of fluorine. Note that it is the opposite of what we observed in P implanted germanium, in which the highest retention was in the hot wafer samples. We speculate that it is because an intertwined implantation generates more defects during implantation (the lower temperature of the substrate yields a lower dynamic annealing), but undergoes a higher thermal budget

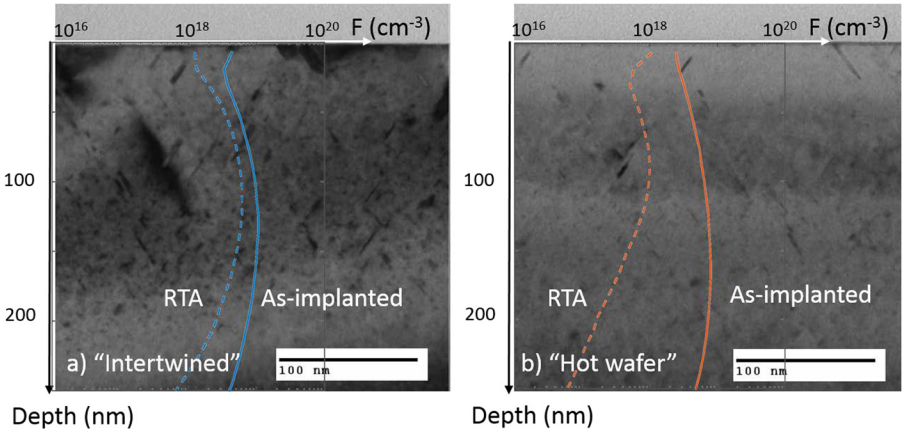

FIG. 4. TEM micrographs (g = 220) with superimposed fluorine SIMS profiles in wafers pre-implanted with NO-dimers. As-implanted (solid line) and post-RTA (dashed line) for a) intertwined and b) hot wafer fluorine implantation ($E_F = 120$ keV, $D_F = 2 \times 10^{14}$ cm^{-2}). The intertwined sample exhibits a higher concentration of defects, which correlates with a higher fraction of retained fluorine post-annealing.

than a hot wafer implantation (it receives multiple RTAs) and therefore also has a more efficient defect removal after implantation. Because O and N react strongly with defects, they stabilize them, and less defects are removed during the RTA than when the more weakly reacting P is present in the sample. As a result, the balance between defect generation and defect removal is different in samples pre-implanted by P or NO dimers, and the net result seems to be more defects in a hot wafer sample for the former, and in an intertwined wafer for the latter.

The low solubility of fluorine is associated with a high diffusivity. Figure 5 shows the fluorine distribution through the whole germanium epi-layer, after a fluorine intertwined implantation (120 keV, 2×10^{14} cm^{-2}) in the NO-dimer pre-implanted sample (as per Fig. 4), for both as-implanted and post- RTA (2 s, 600 °C). We find that while the fluorine concentration is reduced post-RTA in the implanted region (first 200 nm), it increases in the buffer layer at the rear (germanium/silicon) interface. This region is known to contain a high misfit type defect concentration, which results from the lattice and thermal expansion mismatch between silicon and germanium. This suggests that the fluorine undergoes extremely long distance diffusion, with a diffusivity determined to be around 10^{-9} cm^2 s^{-1} (at 600 °C). This value is consistent with estimations from Ref. 39, which yield diffusivities of 10^{-15} cm^2 s^{-1} at 400 °C and $>10^{-13}$ cm^2 s^{-1} at 500 °C. In addition, the concentration of fluorine between 400 nm and 800 nm (where there is no implantation damage, nor misfit dislocations) is below the sensitivity level of our SIMS measurements ($\sim 3 \times 10^{16}$ cm^{-3}), further confirming that fluorine has minimal solubility in high quality crystalline germanium.

Regarding the interaction between fluorine and phosphorus, we have shown earlier (Fig. 3) that a concentration of fluorine at the upper 10^{18} cm^{-3} levels can effectively retard the donor diffusion by passivating vacancies. Despite this, Spreading Resistance Analyses (SRA) have not shown any significant change in the free electron concentration in the implanted region by co-doping with fluorine, as shown in Fig. 6. However, this may not be surprising because the highest concentration of retained fluorine we have been able to achieve, post-RTA, remains below 10^{19} cm^{-3} in samples pre-implanted with phosphorus; too low to affect the electrical activation of 10^{20} cm^{-3} phosphorus.[19] We have observed that the presence of fluorine at these levels does result in a significant (order of magnitude) decrease of the free hole concentration in the non-implanted regions of the layer, which indicates an electrical compensating effect, consistent with the previous work.[40] Given that the p-type character (10^{16} holes cm^{-3}) of the as-grown, un-doped Ge-on-Si layer arises as a result of growth related dislocations, our data indicate that such defects can be effectively passivated by the fluorine. If it can be achieved, increasing the fluorine concentrations in these materials further can provide the opportunity to modify the free carrier concentration in donor co-doped layers.

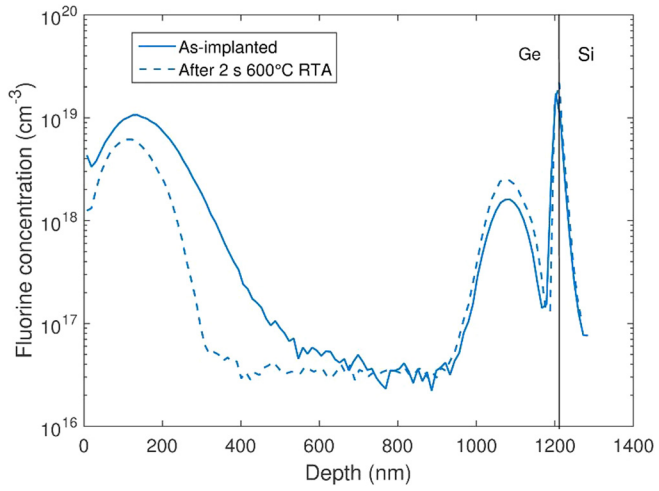

FIG. 5. SIMS fluorine profiles in an intertwined, as-implanted (120 keV, 2×10^{14} cm^{-2}) and annealed (2 s at 600 °C) sample, pre-implanted with NO-dimers. While the concentration of fluorine decreases after RTA around the implantation peak (160 nm), it increases in the misfit dislocated buffer layer at the Si/Ge interface, indicating long distance diffusion. The fluorine sensitivity level of the measurement is $\sim 3 \times 10^{16}$ cm^{-3}.

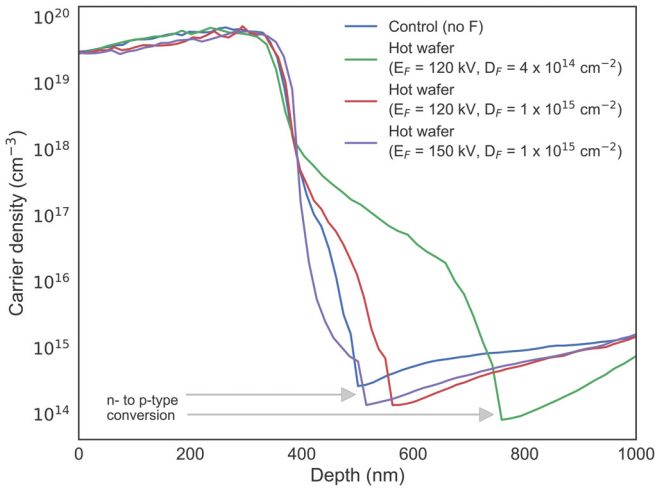

FIG. 6. Free carrier profiles of the hot wafer implanted samples, measured by Spreading Resistance Analysis (SRA). Energy and dose of the fluorine implantations are shown in the legend. The transition from n-type (due to the P implant) to p-type (as-grown material) is reflected by an abrupt change of the derivative of the carrier density. The concentration of fluorine is too low to impact the phosphorus activation in the implanted region, but has a significant effect in the as-grown part of the germanium layer.

CONCLUSIONS

We have implemented two novel, *non-amorphizing* implantation methods to achieve and retain relatively high concentrations of fluorine in germanium: by intertwining low dose implants with RTA, or by implanting directly into a hot wafer, and following with a final RTA. The solubility of fluorine in high quality crystalline germanium is low and mediated by point defects. We find that fluorine exhibits an extremely high diffusivity (10^{-9} cm^2 s^{-1} at 600 °C) in this material and that it can suppress donor diffusion in defective regions through a preferential association with vacancies, without forming complexes with the incorporated donors. The fact that the solubility of fluorine appears to be a strong function of the remnant point defect concentration (post-annealing) means that its retention in sufficiently high concentrations ($>10^{19}$ cm^{-3}) to affect the electrical activation in highly doped n-type germanium is difficult. However, its high diffusivity and affinity with point defects can

be leveraged to decorate specific point defects (in lower concentrations) and spreading defects, such as dislocations associated with growth on lattice mismatched substrates, such as silicon. This can be achieved through long diffusion pathways during relatively short RTA cycles after implanting fluorine outside the active regions of a device, effectively decoupling the implantation from the passivated region.

ACKNOWLEDGMENTS

This work was funded by the *Defense Threat Reduction Agency*, Grant No. *HDTRA1-13-1-0001* and U.S. Air Force Office of Scientific Research Grant (No. FA9550-14-1-0150). C.M. would like to thank Dr. Yan Cai, Dr. Brian Albert, and Mr. Gary Riggott for their help in the growth of the germanium-on-silicon layers. D.P. acknowledges the financial support from the MEC within Programa Nacional de movilidad de recursos humanos del Plan Nacional I+D+i 2008-2011 (EX-2010-0662) and to the program Ramón y Cajal (RYC-2014-16936). H.H.G. acknowledges the support from the Directed Energy Processing Society Graduate Fellowship and the Department of Defense through the National Defense Science and Engineering Graduate Fellowship under Grant No. DGE 0946799. I.F.C. also recognizes the support of MIMIT: Manchester Improving Medicine with Innovation and Technology, as well as the Manchester Academic Health Science Centre (MAHSC). In memory of Professor Russell ('Russ') Gwilliam, a valued colleague, gone too soon.

[1]R. E. Camacho-Aguilera *et al.*, "An electrically pumped germanium laser," Opt. Express **20**(10), 11316–11320 (2012).
[2]R. Koerner *et al.*, "Electrically pumped lasing from Ge Fabry-Perot resonators on Si," Opt. Express **23**(11), 14815 (2015).
[3]G. Dilliway *et al.*, "In situ phosphorus doping of germanium by APCVD," ECS Trans. **3**(7), 599–609 (2006).
[4]H.-Y. Yu *et al.*, "Experimental and theoretical investigation of phosphorus in-situ doping of germanium epitaxial layers," Curr. Appl. Phys. **13**(6), 1060–1063 (2013).
[5]R. E. Camacho-Aguilera, Y. Cai, J. T. Bessette, L. C. Kimerling, and J. Michel, "High active carrier concentration in n-type, thin film Ge using delta-doping," Opt. Mater. Express **2**(11), 1462 (2012).
[6]K. Morii, T. Iwasaki, R. Nakane, M. Takenaka, and S. Takagi, "High performance GeO2/Ge nMOSFETs with source/drain junctions formed by gas phase doping," in Proceedings of the IEEE International Electron Devices Meeting (IEDM) (2009), pp. 1–4.
[7]A. Satta *et al.*, "P implantation doping of Ge: Diffusion, activation, and recrystallization," J. Vac. Sci. Technol. B **24**(1), 494–498 (2006).
[8]E. Simoen *et al.*, "Ion-implantation issues in the formation of shallow junctions in germanium," Mater. Sci. Semicond. Process. **9**(4–5), 634–639 (2006).
[9]M. Koike *et al.*, "Diffusion and activation of n-type dopants in germanium," J. Appl. Phys. **104**(2), 23523 (2008).
[10]J. Coutinho *et al.*, "Strong compensation of n-type Ge via formation of donor–vacancy complexes," Physica B **401–402**, 179–183 (2007).
[11]A. Chroneos, R. W. Grimes, B. P. Uberuaga, S. Brotzmann, and H. Bracht, "Vacancy-arsenic clusters in germanium," Appl. Phys. Lett. **91**(19), 192106 (2007).
[12]A. Chroneos, R. W. Grimes, H. Bracht, and B. P. Uberuaga, "Engineering the free vacancy and active donor concentrations in phosphorus and arsenic double donor-doped germanium," J. Appl. Phys. **104**(11), 113724 (2008).
[13]J. Fage-Pedersen, A. N. Larsen, and A. Mesli, "Irradiation-induced defects in Ge studied by transient spectroscopies," Phys. Rev. B **62**(15), 10116–10125 (2000).
[14]N. S. Patel, C. Monmeyran, A. Agarwal, and L. C. Kimerling, "Point defect states in Sb-doped germanium," J. Appl. Phys. **118**(15), 155702 (2015).
[15]V. P. Markevich, A. R. Peaker, V. V. Litvinov, V. V. Emtsev, and L. I. Murin, "Electronic properties of antimony-vacancy complex in Ge crystals," J. Appl. Phys. **95**(8), 4078–4083 (2004).
[16]V. P. Markevich *et al.*, "Vacancy group-V-impurity atom pairs in Ge crystals doped with P, As, Sb, and Bi," Phys. Rev. B **70**(23), 235213 (2004).
[17]H. Bracht, "Defect engineering in germanium," Phys. Status Solidi A **211**(1), 109–117 (2014).
[18]A. Chroneos, "Defect engineering strategies for germanium," J. Mater. Sci.-Mater. Electron. **24**(6), 1741–1747 (2013).
[19]C. Monmeyran, I. F. Crowe, R. M. Gwilliam, J. Michel, L. C. Kimerling, and A. M. Agarwal, "Strategies for increased donor electrical activity in germanium (opto-) electronic materials: A review," Int. Mater. Rev. **62**(6), 334–347 (2016).
[20]A. Chroneos, R. W. Grimes, and H. Bracht, "Fluorine codoping in germanium to suppress donor diffusion and deactivation," J. Appl. Phys. **106**(6), 63707 (2009).
[21]C. Thomidis *et al.*, "Strong diffusion suppression of low energy-implanted phosphorous in germanium by N-2 co-implantation," ECS Solid State Lett. **4**(6), P47–P50 (2015).
[22]S. Brotzmann *et al.*, "Diffusion and defect reactions between donors, C, and vacancies in Ge. I. Experimental results," Phys. Rev. B **77**(23), 235207 (2008).
[23]M. Shayesteh, V. Djara, M. Schmidt, M. White, A.-M. Kelleher, and R. Duffy, "Fluorine implantation in germanium for dopant diffusion control," AIP Conf. Proc. **1496**, 115–118 (2012).
[24]R. Duffy, M. Shayesteh, M. White, J. Kearney, and A.-M. Kelleher, "The formation, stability, and suitability of n-type junctions in germanium formed by solid phase epitaxial recrystallization," Appl. Phys. Lett. **96**(23), 231909 (2010).
[25]H. A. W. El Mubarek, "Reduction of phosphorus diffusion in germanium by fluorine implantation," J. Appl. Phys. **114**(22), 223512 (2013).
[26]S. Boninelli, G. Impellizzeri, F. Priolo, E. Napolitani, and C. Spinella, "Fluorine in Ge: Segregation and EOR-defects stabilization," Nucl. Instrum. Methods Phys. Res., Sect. B **282**, 21–24 (2012).
[27]G. Impellizzeri *et al.*, "Fluorine effect on As diffusion in Ge," J. Appl. Phys. **109**(11), 113527 (2011).
[28]G. Impellizzeri *et al.*, "Role of F on the electrical activation of As in Ge," ECS J. Solid State Sci. Technol. **1**(3), Q44–Q46 (2012).
[29]D. Pastor *et al.*, "N type doping of strained epitaxial germanium films using ion implantation followed by nanosecond pulse laser melting," MRS Proc. in Program: Symposium GG — Emerging Materials and Platforms for Optoelectronics: MRS, Boston, MA, 30 November-4 December 2015.
[30]G. Hobler and G. Otto, "Status and open problems in modeling of as-implanted damage in silicon," Mater. Sci. Semicond. Process. **6**(1–3), 1–14 (2003).
[31]A. Claverie, S. Koffel, N. Cherkashin, G. Benassayag, and P. Scheiblin, "Amorphization, recrystallization and end of range defects in germanium," Thin Solid Films **518**(9), 2307–2313 (2010).
[32]J. F. Ziegler, M. D. Ziegler, and J. P. Biersack, "SRIM—The stopping and range of ions in matter (2010)," Nucl. Instrum. Methods Phys. Res., Sect. B **268**(11–12), 1818–1823 (2010).
[33]J. B. Liu *et al.*, "Hot implantations of P into Ge: Impact on the diffusion profile," ECS J. Solid State Sci. Technol. **6**(1), P73–P77 (2017).
[34]H.-C. Luan *et al.*, "High-quality Ge epilayers on Si with low threading-dislocation densities," Appl. Phys. Lett. **75**(19), 2909–2911 (1999).
[35]BSTJ, January 1960: "Solid solubilities of impurity elements in germanium and silicon," Standard No. BSTJ 39:1 (Trumbore, F.A.) (1960).
[36]A. Chroneos, B. P. Uberuaga, and R. W. Grimes, "Carbon, dopant, and vacancy interactions in germanium," J. Appl. Phys. **102**(8), 83707 (2007).
[37]A. Chroneos, R. W. Grimes, B. P. Uberuaga, and H. Bracht, "Diffusion and defect reactions between donors, C, and vacancies in Ge. II. Atomistic calculations of related complexes," Phys. Rev. B **77**(23), 235208 (2008).
[38]D. Skarlatos, M. Bersani, M. Barozzi, D. Giubertoni, N. Z. Vouroutzis, and V. Ioannou-Sougleridis, "Nitrogen implantation and diffusion in crystalline germanium: Implantation energy, temperature and Ge surface protection dependence," ECS J. Solid State Sci. Technol. **1**(6), P315–P319 (2012).
[39]D. J. Sprouster *et al.*, "Defect complexes in fluorine-implanted germanium," J. Phys. Appl. Phys. **46**(50), 505310 (2013).
[40]W.-S. Jung, J.-H. Park, A. Nainani, D. Nam, and K. C. Saraswat, "Fluorine passivation of vacancy defects in bulk germanium for Ge metal-oxide-semiconductor field-effect transistor application," Appl. Phys. Lett. **101**(7), 72104 (2012).